



Cite this: *Polym. Chem.*, 2019, **10**, 3163

## Structure and luminescence properties of supramolecular polymers of amphiphilic aromatic thioether–peptide conjugates in water†

Patrick Ahlers,<sup>a</sup> Christian Götz,<sup>b</sup> Steffen Riebe,<sup>c</sup> Michael Zirbes,<sup>a</sup> Matthias Jochem,<sup>a</sup> Daniel Spitzer,<sup>a</sup> Jens Voskuhl,<sup>b</sup> \*c Thomas Basché\*<sup>b</sup> and Pol Besenius<sup>b</sup> \*a

We present the preparation of luminophore–peptide conjugates that self-assemble into supramolecular polymers in neutral buffer. To this end, we have prepared a small library of six conjugates with varying substitution patterns of the aromatic thioethers, as well as varying amino acid sequences. The latter have allowed us to tune the thermodynamic driving force for self-assembly and probe their photoluminescent properties either in the monomeric or polymeric state, while fully avoiding selective solvent techniques or organic solvent mixtures. All of the supramolecular structures were characterised with transmission electron microscopy, circular dichroism measurements, as well as steady-state and time-resolved photoluminescence spectroscopy. In the case of the tetra-substituted (phenylthio)phthalonitrile luminophore we observe a long-lived, red-shifted emission at room temperature which we attribute to phosphorescence upon self-assembly into anisotropic supramolecular polymers. Such an aggregation induced phosphorescence at wavelengths above 600 nm is very promising for the development of tuneable luminophores for applications of multifunctional supramolecular materials in biological systems and time-gated optical microscopy.

Received 2nd December 2018,  
Accepted 23rd April 2019

DOI: 10.1039/c8py01712c

rsc.li/polymers

### Introduction

Supramolecular chemistry excels at producing ordered and nanostructured materials, using reversible and dynamic non-covalent interactions.<sup>1–4</sup> Highly directional supramolecular forces allow the formation of assemblies that range in size, from molecular complexes to polymeric superstructures.<sup>5–11</sup> The unique features of supramolecular materials emerge from the positioning of functional groups into nanoscale objects and are utilized for example in multivalent and multifunctional biomaterials,<sup>12–15</sup> applications in ferromagnetic<sup>16</sup> or paramagnetic<sup>17</sup> materials, and in the design of delivery vehicles with switchable release profiles.<sup>18,19</sup> A recent contribution from our groups, was the application of luminescent

supramolecular polymers, to probe the stability of  $\beta$ -sheet ordered peptide materials in biologically complex media like serum.<sup>20</sup> We made use of luminescent probes that showed an emission in the self-assembled state in water, where the supramolecular organization was switched on, whereas in a water/organic solvent mixture self-assembly was switched off and the characteristic luminescence vanished.<sup>20</sup> This behaviour was reminiscent of the popularised phenomenon of aggregation-induced emission (AIE),<sup>21–23</sup> originally described for flexible siloles and tetraphenylethene derivatives.<sup>24,25</sup> We are most interested in the development of intrinsically luminescent supramolecular polymers that avoid the need for additional labelling of monomers, particularly also luminophores that operate in a photoluminescence “turn-on” fashion. The luminophore we have applied recently is based on an easily accessible 4,5-bis-(phenylthio)phthalonitrile unit, which was equipped with a  $\beta$ -sheet encoded alternating phenyl alanine-histidine peptide sequence (FHFHF) and a C-terminal charged dendron. We assigned the induced luminescent increase in the supramolecular polymers to a combination of restricted intramolecular motion (RIM)<sup>26</sup> and twisted intramolecular charge transfer (TICT).<sup>27</sup> However, like in the large majority of reported examples of materials that make use of aggregation induced emission properties, we heavily relied on switching

<sup>a</sup>Institute of Organic Chemistry, Johannes Gutenberg-University Mainz, Duesbergweg 10-14, 55128 Mainz, Germany. E-mail: besenius@uni-mainz.de

<sup>b</sup>Institute of Physical Chemistry, Johannes Gutenberg-University Mainz, Duesbergweg 10-14, 55128 Mainz, Germany. E-mail: thomas.basche@uni-mainz.de

<sup>c</sup>Institute of Organic Chemistry, University of Duisburg-Essen, Universitätsstrasse 7, 45117 Essen, Germany. E-mail: jens.voskuhl@uni-due.de

†Electronic supplementary information (ESI) available: Experimental procedures, materials and methods, detailed synthetic procedures and the characterization of all molecules. See DOI: 10.1039/c8py01712c

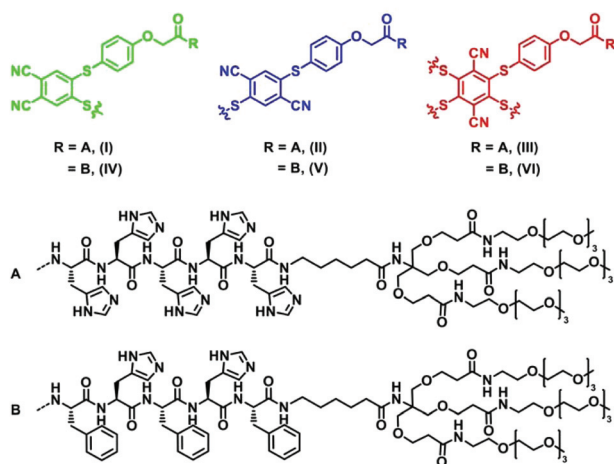


**Fig. 1** Chemical structures of the  $\beta$ -sheet encoded amphiphilic (phenylthio)phthalonitrile luminophores I–VI, using histidine (H) and phenylalanine (F) peptides HHHHH (sequence A) and FHFHF (sequence B) linked to a hydrophilic dendritic tetraethylene glycol.

solvent polarities to turn the supramolecular polymerisation “on” and “off”, thus changing both the self-assembly state as well as the dielectric constant of the medium. The latter is further known to induce solvatochromic behaviour.

In order to probe the photoluminescent properties of supramolecular polymers using tailor-made luminophores we designed a small library of six new amphiphilic peptide conjugates (Fig. 1) that can be probed in pure aqueous buffer and avoid the addition of organic solvents. We were especially interested in using (phenylthio)phthalonitrile type luminophores that can exhibit phosphorescent properties with large Stokes shifts and emission wavelengths in the near infra-red regime.<sup>28</sup>

## Experimental section

Experimental procedures, materials and methods, detailed synthetic procedures and the characterization of all molecules are provided in the ESI.†

NMR-spectra were recorded on a BRUKER ARX 300 spectrometer, BRUKER Avance II 400 and BRUKER Avance III 600 spectrometer; mass spectra were recorded on the electrospray ionization spectrometer (ESI) QToF Ultima 3 (micromass/Waters) using methanol as solvent. Molecules of a high molecular mass were detected using matrix assisted laser desorption ionization-time of flight (MALDI-ToF) spectrometry using a Shimadzu Axima CFR.

For negative stain TEM, 5  $\mu$ L sample droplets were adsorbed for 1 min on freshly glow-discharged copper grids covered by a thin, continuous carbon film (Electron Microscopy Sciences; CF300-CU). The grids were then negatively stained with 2.0% uranyl acetate (Polysciences) for 15 s before blotting with filter papers (Whatman no. 4). All images were recorded with a FEI Tecnai T12 electron microscope equipped with a LaB<sub>6</sub>-cathode and operated at 120 kV. Digital electron images were recorded

with a 4k  $\times$  4k complementary metal–oxide–semiconductor (CMOS) camera (TVIPS) under minimal dose conditions.

CD spectra were recorded on a J-815 (JASCO) using the software Spectra Manager 2.08.04 and processed with Origin Pro 9.1 G. All spectra were recorded at 20  $^{\circ}$ C with a total monomer concentration of 60  $\mu$ M in sodium phosphate buffer using quartz cells with a path length of 2 mm. The low monomer concentrations made sure that the high tension (HT) voltage was lower than 600 V at all times. All spectra were corrected by subtraction of the background (buffer).

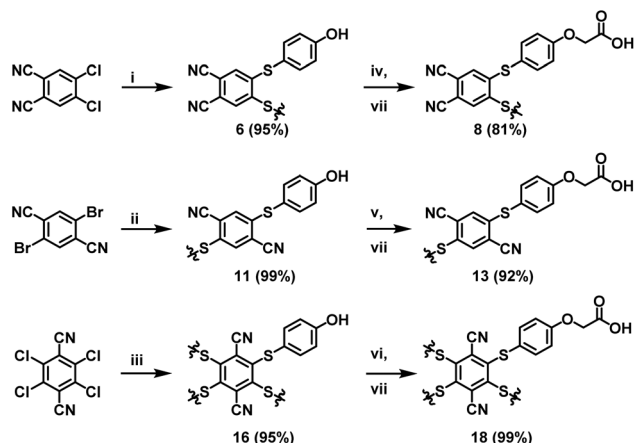
Absorption spectra were taken at room temperature with an UV/Vis spectrophotometer (Lambda 850, PerkinElmer). For photoluminescence spectra and decay curves, 2 mL of sample were measured in quartz fluorescence cuvettes. The samples were degassed by bubbling argon *via* a syringe through the solution. The luminescence spectra were taken at room temperature in a 90 $^{\circ}$  geometry using a spectrofluorometer (Fluorolog-3, Horiba Jobin Yvon). Excitation slit widths were set to 5 nm, while the emission slit width was 1 nm. Time-resolved photoluminescence measurements were performed with a Fluorolog-3 spectrofluorometer equipped with a FluoroHub TCSPC unit (Horiba Jobin Yvon); for further details see ESI.†

## Results and discussion

### Structural design and synthesis

The building block design is based on three different aromatic thioether luminophores,<sup>28–30</sup> which have previously been shown to give rise to enhanced photoluminescent properties upon aggregation in DMF/H<sub>2</sub>O mixtures.<sup>28</sup> The carboxylic acid bearing functional aromatic thioethers **8**, **13** and **18** were obtained in three high yield synthetic steps starting from 4,5-dichlorophthalonitrile, 2,5-dibromophthalonitrile or 2,3,5,6-tetrachloroterephthalonitrile respectively (Scheme 1).

We chose two different peptide amphiphile motifs to prepare the luminophore–peptide conjugates. Using the  $\beta$ -sheet encoded, phenylalanine(F)–histidine(H) peptide sequence FHFHF linked to a hydrophilic Newkome-based dendritic tetraethylene glycol unit (**2**, see ESI†), we have previously shown that one-dimensional nanorods are obtained with high degrees of order in the hydrophobic core of the nanostructures.<sup>31</sup> We further used the complementary pentahistidine peptide amphiphile (**5**), which is considerably more hydrophilic and reduces the driving force for supramolecular polymerisation in water. The oligopeptides Fmoc-FHFHF-OH and Fmoc-HHHHH-OH were synthesised *via* solid phase peptide synthesis (SPPS) using the Fmoc-strategy and were coupled to the hydrophilic dendritic unit *via* PyBOP mediated peptide coupling using HOAt as an additive to avoid epimerization. The detailed synthetic steps, reaction conditions and molecular characterizations are described in the ESI.† After Fmoc-deprotection the peptide amphiphiles **2** and **5** were coupled to the carboxylic acid bearing aromatic thioethers **8**, **13** and **18** in high yielding PyBOP mediated couplings (78%–99%) to yield the protected peptide amphiphiles **9**, **10**, **14**, **15**,



**Scheme 1** Synthesis of the carboxylic acid bearing functional aromatic thioethers **8**, **13** and **18**: (i) 4,5-Dichlorophthalonitrile (1.0 eq.), 4-mercaptophenol (3.0 eq.),  $K_2CO_3$  (6.0 eq.), 80 °C, DMF, 1 d, 95%; (ii) 2,5-dibromophthalonitrile (1.0 eq.), 4-mercaptophenol (4.6 eq.),  $K_2CO_3$  (6.0 eq.), 45 °C, DMF, 6 h, 99%; (iii) 2,3,4,5-tetrachlorophthalonitrile (1.0 eq.), 4-mercaptophenol (5.8 eq.),  $K_2CO_3$  (12.1 eq.), 45 °C, DMF, 6 h, 94%; (iv) **6** (1.0 eq.), bromo *tert*-butyl acetic acid (5.7 eq.),  $K_2CO_3$  (18.9 eq.), KI (cat.), 60 °C, DMF, 48 h, 83%; (v) **11** (1.0 eq.), bromo *tert*-butyl acetic acid (3.0 eq.),  $K_2CO_3$  (6.0 eq.), 40 °C, DMF, 24 h, 92%; (vi) **16** (1.0 eq.), bromo *tert*-butyl acetic acid (12.0 eq.),  $K_2CO_3$  (53.0 eq.), 40 °C, DMF, 24 h, 99%; (vii) **7/12/17**, DCM/TFA (15 : 4), RT, 6 h, 81%/92%/99%.

**19** and **20**. After TFA mediated acidic deprotection of the trityl protected histidine side chains, the HHHHH encoded water soluble peptide–luminophore conjugates **I**, **II** and **III**, and the complementary FHFHF building blocks **IV**, **V** and **VI** were finally obtained, with molecular weights between  $3864 \text{ g mol}^{-1}$  and  $7695 \text{ g mol}^{-1}$  depending on the peptide sequence and degree of substitution in the hydrophobic phthalonitrile core. These molecular units were ready to be investigated for their self-assembly behaviour using transmission electron microscopy (TEM), circular dichroism (CD) and photoluminescence spectroscopy.

#### Investigation of the supramolecular assemblies using TEM microscopy and CD spectroscopy

The substitution pattern in the 2,5-bis-(phenylthio)phthalonitrile and 2,3,4,5-tetra-(phenylthio)phthalonitrile leads to peptide conjugates with a bolaamphiphilic structure in **II** and **III**, **V** and **VI**. On the other hand, the 4,5-bis-(phenylthio)phthalonitrile core yields facial amphiphiles **I** and **IV**. We expected the main driving force for supramolecular polymerisation to originate from the  $\beta$ -sheet encoded phenylalanine and/or histidine peptide sequences. In order to investigate the morphology of all the peptide amphiphile conjugates **I–VI**, we carried out negative stain TEM experiments (Fig. 2 and S4†).<sup>32</sup> The solu-

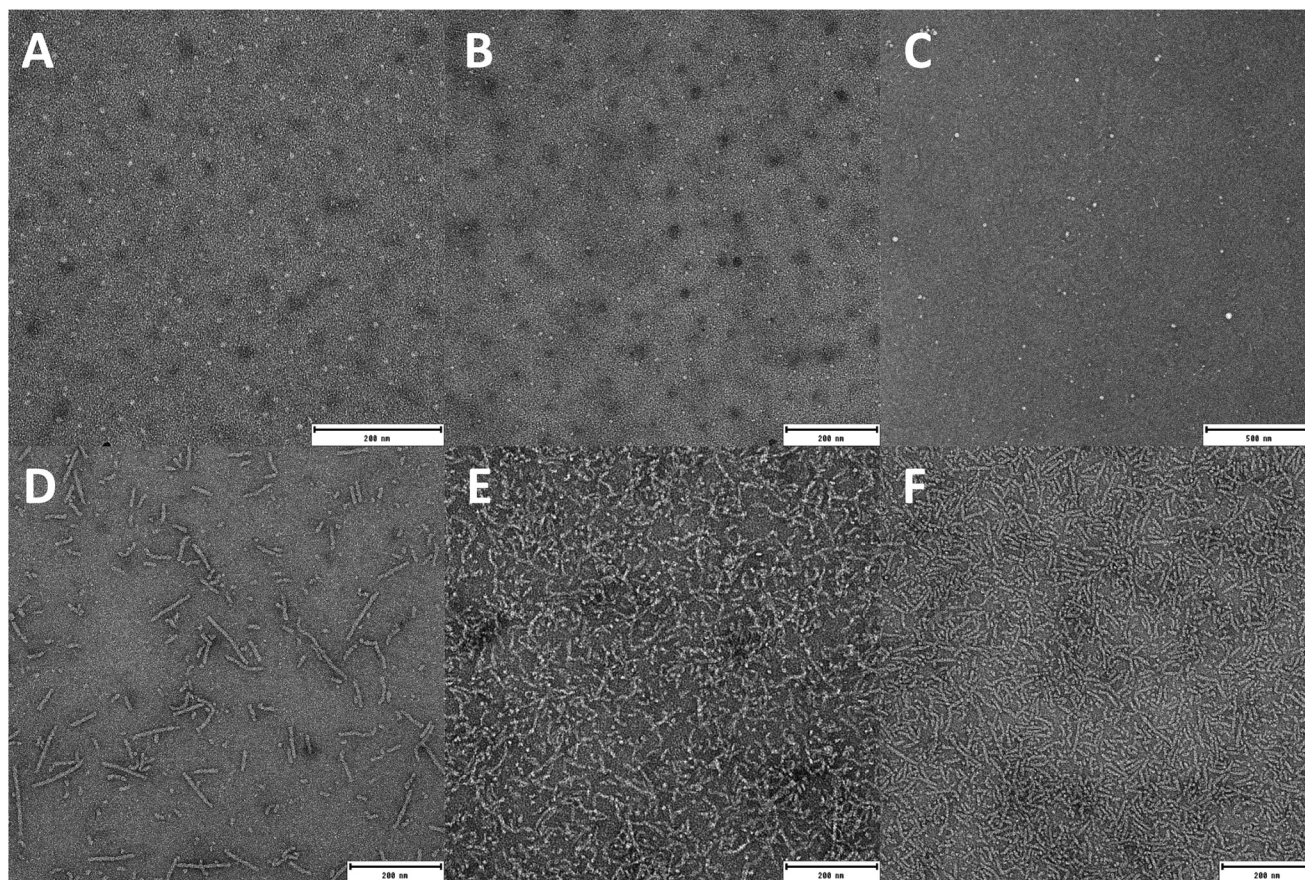


**Fig. 2** Negative stained TEM images of luminophores **I** (A), **II** (B), **III** (C), **IV** (D), **V** (E) and **VI** (F), all obtained from solutions prepared using  $50 \mu\text{M}$  monomer concentrations in 10 mM TRIS buffer (pH 7.4) at 20 °C. Scale bars A, B, D–F: 200 nm; C: 500 nm.

tions of the HHHHH sequenced luminophore conjugates **I–III** at 50  $\mu\text{M}$  concentrations in TRIS buffer (10 mM) at pH 7.4, all showed only very small spherical objects, with diameters of about 7.5 nm for **I** and **II**, and 15 nm for **III**. In the latter case, the chain extended length of a single molecule, including the terminal tetraethylene glycol chains corresponds to about 12 nm. We therefore assign the spherical objects to isolated molecules. Alternatively, very small oligomers with a micellar morphology would also be possible. This result is slightly surprising given that even at pH 7.4, where all the imidazole functional groups in the side chains are deprotonated,<sup>31</sup> the hydrophobic core and peptide sequence does not seem to induce anisotropic growth into supramolecular polymers. In contrast, when the HHHHH sequence is changed to a more hydrophobic FHFHF sequence, all building blocks **IV**, **V** and **VI** lead to anisotropic 1D morphologies. Self-assembled flexible rods are obtained with a thickness of  $15 \text{ nm} \pm 2.5 \text{ nm}$  and an average length of  $47 \text{ nm} \pm 12 \text{ nm}$ ,  $55 \text{ nm} \pm 10 \text{ nm}$  and  $45 \text{ nm} \pm 13 \text{ nm}$  for self-assembled **IV**, **V** and **VI**, respectively (Fig. S4†). These observations are in agreement with the previously reported cationic rod-like micelles based on a derivative of amphiphile **IV**.<sup>20</sup> We suggest that the semi-flexible rods are best described as micellar-like morphologies with the hydrophobic block of the amphiphiles pointing into the core of one-dimensional assemblies, which are solvated *via* the tetraethylene glycol dendrons in the shell.

CD spectroscopy has been a powerful tool to investigate the thermodynamic and kinetic driving force in supramolecular polymers based on peptide monomers.<sup>33–35</sup> In order to corroborate the morphological investigations of the six different amphiphiles in aqueous buffer, we probed CD spectra of all the luminophore–peptide conjugates **I–VI**, at a monomer concentration of 50  $\mu\text{M}$  in 10 mM sodium phosphate buffer (pH 7.4) at 20 °C (Fig. 3). The HHHHH containing peptide amphiphiles **I**, **II** and **III** fail to give rise to strong CD effects. The spectra indicate the presence of a negative band just below  $\lambda = 200 \text{ nm}$ , which is usually assigned to peptides in the random coil conformation. In addition, building block **I** shows a very weak positive band at  $\lambda = 220 \text{ nm}$  and building block **III** two weak positive bands at  $\lambda = 205 \text{ nm}$  and  $225 \text{ nm}$ , and a negative band at  $\lambda = 250 \text{ nm}$ . The aqueous solutions of compounds **IV–VI** are significantly different. In all cases strong negative CD bands appear at  $\lambda = 215 \text{ nm}$ ,  $245 \text{ nm}$  and  $280 \text{ nm}$  for **IV**,  $\lambda = 215 \text{ nm}$ ,  $240 \text{ nm}$  and  $300 \text{ nm}$  for **V**, and  $\lambda = 200 \text{ nm}$ ,  $215 \text{ nm}$ ,  $240 \text{ nm}$  and  $265 \text{ nm}$  in the case of **VI**. In combination with the conclusions drawn from TEM experiments, the CD spectroscopic investigations show complementary evidence that the oligohistidine peptide amphiphiles are too hydrophilic to lead to larger aggregates in aqueous buffer. In contrast, the peptide sequence FHFHF is much more hydrophobic and leads to ordered assemblies, as indicated by the pronounced CD effects, with a 1D morphology most likely due to the high directionality of the hydrogen bond encoded peptides. In addition, all self-assembled amphiphiles **IV–VI** give rise to different characteristic CD bands, depending on the geometry and substitution pattern of the (phenylthio)phthalonitrile based hydrophobic core.

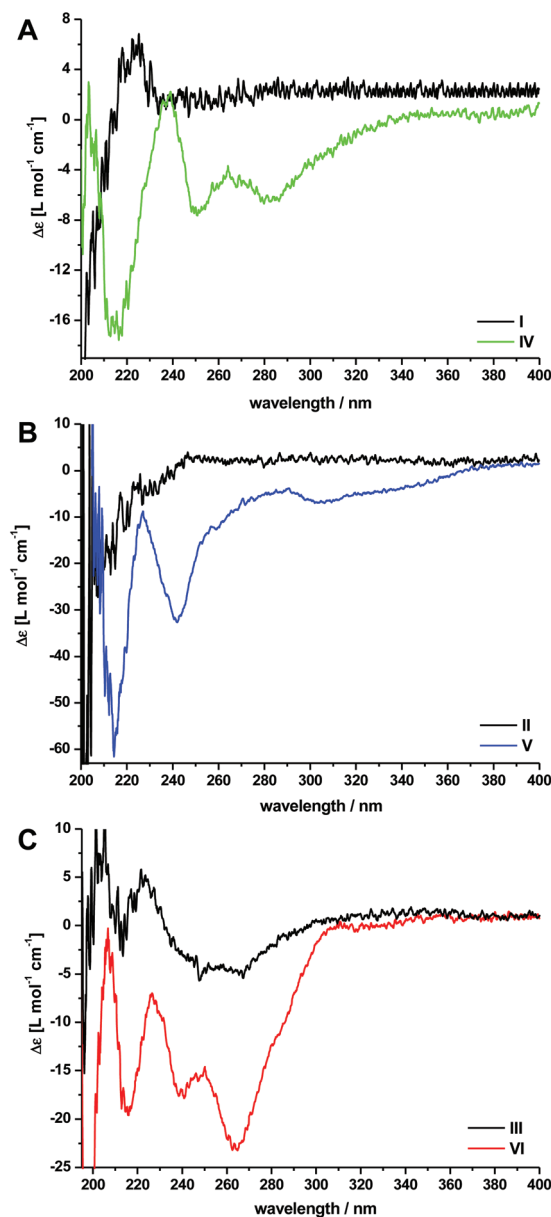


Fig. 3 CD spectra of luminophores **I** and **IV** (A), **II** and **V** (B), **III** and **VI** (C) at monomer concentrations of 50  $\mu\text{M}$  in 10 mM sodium phosphate buffer (pH 7.4) at 20 °C. Monomeric solutions are shown in black and polymeric structures as coloured lines in the graphs.

### Investigation of the supramolecular assemblies using photoluminescence spectroscopy

Due to the previously observed luminescence of a cationic derivative of 4,5-bis-(phenylthio)phthalonitrile substituted  $C_2$ -symmetrical peptide amphiphile **IV**,<sup>20</sup> we pursued systematic UV/Vis and photoluminescence spectroscopy experiments in order to be able to clearly differentiate the emissive properties of all (phenylthio)phthalonitrile luminophores in the molecular dissolved and self-assembled nanostructured state. The UV/Vis absorption spectra of the molecularly dissolved (phenylthio)phthalonitrile core gives rise to absorption bands between 250 nm and 500 nm (Fig. S1–S3†). While the absorp-

tion spectra of **III** and **VI** are very similar, in the case of the supramolecular polymers of **IV** and **V**, specific absorption bands are not visible due to strong scattering contributions from the solutions.

The emission spectra of compounds **I–VI** in 10 mM sodium phosphate buffer (pH 7.4) under inert argon atmosphere are shown in Fig. 4. The small shoulder in all spectra at  $\lambda = 425$  nm is assigned to the inelastic Raman scattering peak of the excitation light at 370 nm. Notably, fluorescence emission

is observed for all species, even though in a recent study we have reported that similar thioethers did not show emission in the molecularly dissolved state in DMF<sup>28</sup> or in DMSO.<sup>20</sup> Possible explanations for this difference include the formation of small spherical aggregates in water even in the case of **I–III**. In order to investigate possible oligomerisation, we performed diffusion ordered <sup>1</sup>H-NMR-spectroscopy experiments<sup>33</sup> of molecule **III** in a solvent prone to induce disassembly, as well as in water. The diffusion coefficient  $D$  of **III** in DMSO- $d_6$  was  $7.2 \times 10^{-11} \text{ m}^2 \text{ s}^{-1}$ , and  $1.0 \times 10^{-10}$  in D<sub>2</sub>O (Fig. S5–S6†). The calculated hydrodynamic radii  $R_H$  were 1.4 nm in DMSO- $d_6$  and 1.9 nm for D<sub>2</sub>O (Table S2†). The latter value matches previously reported  $R_H$  values for molecularly dissolved monomers of similar molar mass, which were obtained from dynamic light scattering experiments in aqueous buffer.<sup>36</sup> We can therefore exclude that the emission at  $\lambda_{\text{em}} = 460$  nm observed for **III**, is due to oligomerisation or micelle formation. The pentahistidine peptide sequences HHHHH, which were also incorporated in the amphiphiles **I** and **II**, are too hydrophilic to induce oligomerisation in aqueous buffer, as already suggested by TEM and CD spectroscopy experiments. Alternatively, one could imagine that in the molecularly dissolved state the peptide side-arms are collapsed, shielding the (phenylthio)phthalonitrile core and thus preventing exposure of the luminophores to the polar environment in the aqueous phase.

We point out that for **IV** and **V** we did not observe a significant change in the photoluminescence in the self-assembled state compared to the molecular dissolved state (**I**, **II**). In particular, only minor differences in the band intensities and widths are observed. A common observation for organic fluorophores is that the fluorescence quantum yield decreases due to self-quenching or other quenching phenomena upon aggregation.<sup>37</sup> For the disubstituted (phenylthio)phthalonitrile hydrophobic cores in **IV** and **V**, theoretical calculations have suggested that the Stokes shifts of more than 80 nm are most likely caused by geometrical twists upon electronic excitation of the thioaryl substituents around the C–S single bonds linking the electron rich alkoxy substituted and the electron poor nitrile substituted aromatic rings.<sup>28</sup> The emission from such systems is best described to originate from a twisted intramolecular charge-transfer state (TICT).<sup>38</sup> It appears that also in the self-assembled nanostructured state (**IV**, **V**), the TICT-type emission prevails. The hypsochromic shift of **V** might indicate some conformational restriction in the supramolecular structure induced by packing of the luminophore into a hydrophobic self-assembled domain of the rod-like micelles of **V**. The amphiphile **VI** behaves strikingly different compared to **IV** and **V**. In the supramolecular polymeric state, a strong new emission band appears at  $\lambda_{\text{em}} = 615$  nm in addition to the band at  $\lambda_{\text{em}} = 460$  nm ( $\lambda_{\text{exc}} = 370$  nm).

To get further insight into the nature of the emissive states, we performed photoluminescence (PL) lifetime experiments with a time-correlated single photon counting (TCSPC) set-up. The PL decays of **I–III** could be satisfactorily fitted by a bi-exponential function, yielding intensity weighted average fluo-

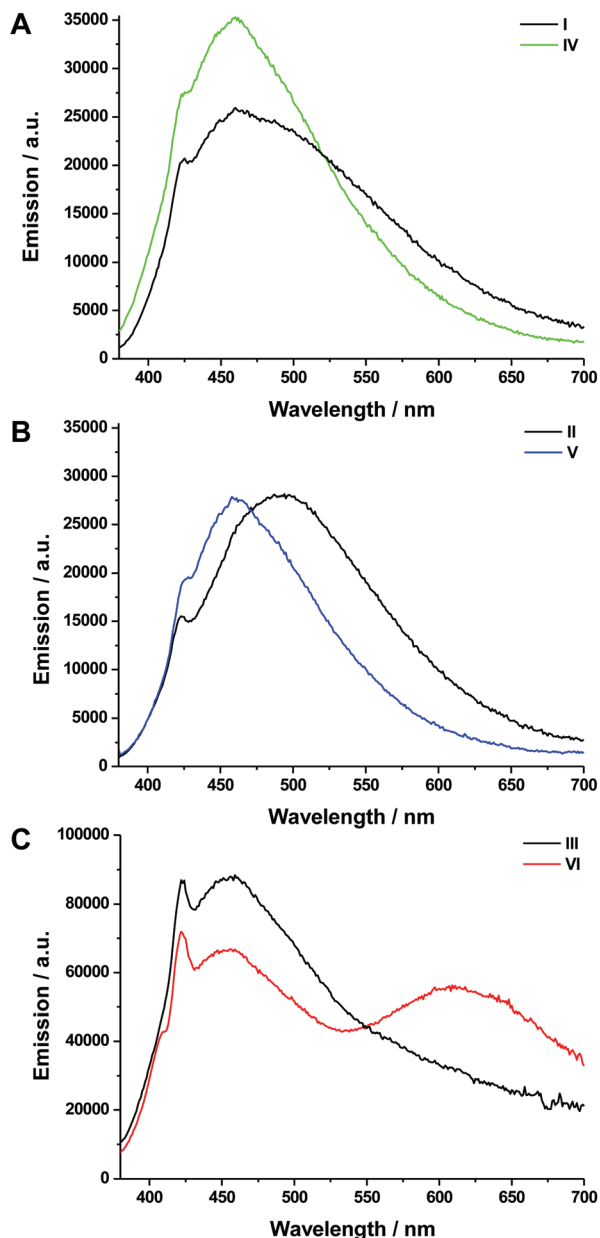


Fig. 4 Photoluminescence spectroscopic measurements of luminophores **I–VI** in 10 mM sodium phosphate buffer (pH 7.4) at 20 °C using an excitation wavelength of  $\lambda_{\text{exc}} = 370$  nm. The monomer concentrations for the conjugates **I** and **IV** were 37.5  $\mu\text{M}$  (graph A), for **II** and **V** 12.5  $\mu\text{M}$  (graph B) and for **III** and **VI** 9.4  $\mu\text{M}$  (graph C). The monomeric solutions are shown in black and the polymeric structures as coloured lines in the graphs.

rescence lifetimes  $\tau$  between 2.3 ns and 3.6 ns (see ESI, Table 1†), which are typical of small organic fluorophores. In accordance with their comparable spectral shapes and positions, **IV** and **V** gave rise to lifetimes  $\tau$  in the same time range as **I–III** (see ESI, Table 1†). The PL decay of **VI** – recorded at an emission wavelength of 615 nm – was fitted using a tri-exponential function. Since at the detection wavelength of 615 nm there is still appreciable cross-talk from the emission at 460 nm, we used the PL lifetimes from the bi-exponential decay of **III** and kept them fixed while fitting the decay (see ESI, Table 1†). Following this procedure, we found a third decay component with a life time of 337 ns which originates from the red emission at 615 nm in the self-assembled state (**VI**). We attribute this long-lived emission to phosphorescence from the triplet state  $T_1$  as has been reported for aromatic thioethers in a strongly aggregated state.<sup>28</sup> This view is supported by the decrease of the red PL under ambient conditions, when  $T_1$  is quenched by the presence of ground state oxygen. At present we are unable to assign the long-lived emission to originate either from localized excitations or from excimers,<sup>39–44</sup> which appear to be a reasonable option in the self-assembled state. Furthermore, an increase of the substitution pattern from two (**I**, **IV** and **II**, **V**) to four thioethers (**III**, **VI**) increases the probability for spin-forbidden singlet–triplet transitions due to the heavy-atom effect. The observation of phosphorescence in **VI** (and its absence in **III**) may again be related to conformational restrictions in the self-assembled nanostructured state, which increase the likelihood of long-lived, radiative phosphorescence transitions.

In summary, our specifically designed peptide–luminophore conjugates are an important addition to the field of luminescent probes that are emissive in the self-assembled state and operate *via* the popularized aggregation-induced emission mechanism. They are operative in purely aqueous environments, do not require selective solvent techniques and will be much easier implemented in applications under biologically relevant conditions.

## Conclusions

To conclude, we have synthesised a small library of three (phenylthio)phthalonitrile luminophores conjugated with two different peptide amphiphiles. Using these six conjugates we were able to probe their structures and photoluminescent properties using a combination of TEM, CD and optical spectroscopy. The HHHHH containing peptide amphiphiles **I**, **II** and **III**, fail to induce supramolecular polymerisation. On the other hand, the more hydrophobic peptide sequence FHFHF leads to ordered assemblies with a 1D morphology for the luminophore–peptide conjugates **IV**, **V** and **VI**. In TEM images, the 1D supramolecular polymers from the substituted 2,5-bis-(phenylthio)phthalonitrile and 2,3,4,5-tetra-(phenylthio)phthalonitrile bolaamphiphiles **V** and **VI** seem slightly more flexible than the morphologies obtained from the 4,5-bis-(phenylthio)phthalonitrile substituted facial amphiphile **IV**. However, the

average length of the self-assembled flexible rods does not depend on the substitution pattern or degree of substitution for the three molecular building blocks. In none of the three different amphiphiles the emission is quenched in the self-assembled state. Most remarkably, we were able to identify a tetra-substituted (phenylthio)phthalonitrile-peptide conjugate **VI** which in the supramolecular polymer state shows a large bathochromic shift compared to the monomeric molecularly dissolved state. The emission at a wavelength of 615 nm is not observed for conjugates **IV** and **V**, and most probably originates from a triplet excited state with a life time close to 0.5  $\mu$ s. Given that the luminophore **VI** contains four thioethers compared to only two thioethers for **IV** and **V**, we attribute the observed phosphorescence to the increased probability for spin-forbidden singlet–triplet transitions due to the heavy-atom effect. These results are promising for the development of aggregation-induced phosphorescent organic emitters, and for the study of the assembly state of (bio)supramolecular systems, particularly in view of probing and tracking the peptide materials in complex biological media, using for example gated-detection microscopes.

## Conflicts of interest

There are no conflicts to declare.

## Acknowledgements

We acknowledge Mrs Katrin Stamer for her help with the synthesis of the luminophores. J. V. acknowledges the “Fonds der chemischen Industrie” (FCI) for financial support. T. B. and P. B. are grateful for financial support from CINEMA and LESSING Impuls Fonds (Johannes Gutenberg-University of Mainz).

## References

- 1 T. Aida, E. W. Meijer and S. I. Stupp, *Science*, 2012, **335**, 813–817.
- 2 S. T. Ryan, R. M. Young, J. J. Henkelis, N. Hafezi, N. A. Vermeulen, A. Hennig, E. J. Dale, Y. Wu, M. D. Krzyaniak, A. Fox, W. M. Nau, M. R. Wasielewski, J. F. Stoddart and O. A. Scherman, *J. Am. Chem. Soc.*, 2015, **137**, 15299–15307.
- 3 J.-F. Lutz, J.-M. Lehn, E. W. Meijer and K. Matyjaszewski, *Nat. Rev. Mater.*, 2016, **1**, 16024.
- 4 D. B. Amabilino, D. K. Smith and J. W. Steed, *Chem. Soc. Rev.*, 2017, **46**, 2404–2420.
- 5 T. F. A. de Greef, M. M. J. Smulders, M. Wolffs, A. P. H. J. Schenning, R. P. Sijbesma and E. W. Meijer, *Chem. Rev.*, 2009, **109**, 5687–5754.
- 6 Z. Liu, G. Liu, Y. Wu, D. Cao, J. Sun, S. T. Schneebeli, M. S. Nassar, C. A. Mirkin and J. F. Stoddart, *J. Am. Chem. Soc.*, 2014, **136**, 16651–16660.

- 7 A. Samanta and B. J. Ravoo, *Angew. Chem., Int. Ed.*, 2014, **53**, 12946–12950.
- 8 J.-M. Lehn, *Angew. Chem., Int. Ed.*, 2015, **54**, 3276–3289.
- 9 Y. Liu, M. C. A. Stuart, E. Buhler, J.-M. Lehn and A. K. H. Hirsch, *Adv. Funct. Mater.*, 2016, **26**, 6297–6305.
- 10 F. Würthner, *Acc. Chem. Res.*, 2016, **49**, 868–876.
- 11 E. Krieg, M. M. C. Bastings, P. Besenius and B. Rybtchinski, *Chem. Rev.*, 2016, **116**, 2414–2477.
- 12 K. Petkau-Milroy and L. Brunsveld, *Org. Biomol. Chem.*, 2013, **11**, 219–232.
- 13 J. Cabanas-Danés, E. D. Rodrigues, E. Landman, J. van Weerd, C. van Blitterswijk, T. Verrips, J. Huskens, M. Karperien and P. Jonkheijm, *J. Am. Chem. Soc.*, 2014, **136**, 12675–12681.
- 14 M. J. Webber, E. A. Appel, E. W. Meijer and R. Langer, *Nat. Mater.*, 2016, **15**, 13–26.
- 15 O. J. G. M. Goor, S. I. S. Hendrikse, P. Y. W. Dankers and E. W. Meijer, *Chem. Soc. Rev.*, 2017, **46**, 6621–6637.
- 16 A. S. Tayi, A. K. Shveyd, A. C. H. Sue, J. M. Szarko, B. S. Rolczynski, D. Cao, T. J. Kennedy, A. A. Sarjeant, C. L. Stern, W. F. Paxton, W. Wu, S. K. Dey, A. C. Fahrenbach, J. R. Guest, H. Mohseni, L. X. Chen, K. L. Wang, J. F. Stoddart and S. I. Stupp, *Nature*, 2012, **488**, 485–489.
- 17 P. Besenius, J. L. M. Heynens, R. Straathof, M. M. L. Nieuwenhuizen, P. H. H. Bomans, E. Terreno, S. Aime, G. J. Strijkers, K. Nicolay and E. W. Meijer, *Contrast Media Mol. Imaging*, 2012, **7**, 356–361.
- 18 P. Zhang, A. G. Cheetham, Y.-a. Lin and H. Cui, *ACS Nano*, 2013, **7**, 5965–5977.
- 19 Y. Qian and J. B. Matson, *Adv. Drug Delivery Rev.*, 2017, **110–111**, 137–156.
- 20 H. Frisch, D. Spitzer, M. Haase, T. Basche, J. Voskuhl and P. Besenius, *Org. Biomol. Chem.*, 2016, **14**, 5574–5579.
- 21 J. Liang, B. Z. Tang and B. Liu, *Chem. Soc. Rev.*, 2015, **44**, 2798–2811.
- 22 S. Xu, Y. Yuan, X. Cai, C.-J. Zhang, F. Hu, J. Liang, G. Zhang, D. Zhang and B. Liu, *Chem. Sci.*, 2015, **6**, 5824–5830.
- 23 A. Han, H. Wang, R. T. K. Kwok, S. Ji, J. Li, D. Kong, B. Z. Tang, B. Liu, Z. Yang and D. Ding, *Anal. Chem.*, 2016, **88**, 3872–3878.
- 24 J. Luo, Z. Xie, J. W. Y. Lam, L. Cheng, H. Chen, C. Qiu, H. S. Kwok, X. Zhan, Y. Liu, D. Zhu and B. Z. Tang, *Chem. Commun.*, 2001, 1740–1741.
- 25 J. Mei, N. L. C. Leung, R. T. K. Kwok, J. W. Y. Lam and B. Z. Tang, *Chem. Rev.*, 2015, **115**, 11718–11940.
- 26 J. Mei, Y. Hong, J. W. Y. Lam, A. Qin, Y. Tang and B. Z. Tang, *Adv. Mater.*, 2014, **26**, 5429–5479.
- 27 W. Rettig, *Angew. Chem., Int. Ed. Engl.*, 1986, **25**, 971–988.
- 28 S. Riebe, C. Vallet, F. v. d. Vight, D. Gonzalez-Abadelo, C. Wölper, C. A. Strassert, G. Jansen, S. Knauer and J. Voskuhl, *Chem. – Eur. J.*, 2017, **23**, 13660–13668.
- 29 J. Stelzer, C. Vallet, A. Sowa, D. Gonzalez-Abadelo, S. Riebe, C. G. Daniliuc, M. Ehlers, C. A. Strassert, S. K. Knauer and J. Voskuhl, *ChemistrySelect*, 2018, **3**, 985–991.
- 30 H. Matthias, R. Steffen and V. Jens, *Chem. – Eur. J.*, 2018, **24**, 12221–12230.
- 31 P. Ahlers, H. Frisch, R. Holm, D. Spitzer, M. Barz and P. Besenius, *Macromol. Biosci.*, 2017, **17**, 1700111.
- 32 H. Frisch, Y. Nie, S. Raunser and P. Besenius, *Chem. – Eur. J.*, 2015, **21**, 3304–3309.
- 33 R. Appel, J. Fuchs, S. M. Tyrrell, P. A. Korevaar, M. C. A. Stuart, I. K. Voets, M. Schönhoff and P. Besenius, *Chem. – Eur. J.*, 2015, **21**, 19257–19264.
- 34 F. Tantakitti, J. Boekhoven, X. Wang, R. V. Kazantsev, T. Yu, J. Li, E. Zhuang, R. Zandi, J. H. Ortony, C. J. Newcomb, L. C. Palmer, G. S. Shekhawat, M. O. de la Cruz, G. C. Schatz and S. I. Stupp, *Nat. Mater.*, 2016, **15**, 469–476.
- 35 B. Kemper, L. Zengerling, D. Spitzer, R. Otter, T. Bauer and P. Besenius, *J. Am. Chem. Soc.*, 2018, **140**, 534–537.
- 36 P. Ahlers, K. Fischer, D. Spitzer and P. Besenius, *Macromolecules*, 2017, **50**, 7712–7720.
- 37 J. R. Lakowicz, *Principles of Fluorescence Spectroscopy*, Springer, 3rd edn, 2006.
- 38 Z. R. Grabowski, K. Rotkiewicz and W. Rettig, *Chem. Rev.*, 2003, **103**, 3899–4032.
- 39 F. M. Winnik, *Chem. Rev.*, 1993, **93**, 587–614.
- 40 R. F. Fink, J. Seibt, V. Engel, M. Renz, M. Kaupp, S. Lochbrunner, H.-M. Zhao, J. Pfister, F. Würthner and B. Engels, *J. Am. Chem. Soc.*, 2008, **130**, 12858–12859.
- 41 H. Yoo, J. Yang, A. Yousef, M. R. Wasielewski and D. Kim, *J. Am. Chem. Soc.*, 2010, **132**, 3939–3944.
- 42 X. Zhang, D. Görl, V. Stepanenko and F. Würthner, *Angew. Chem., Int. Ed.*, 2014, **53**, 1270–1274.
- 43 Q. Li and Z. Li, *Adv. Sci.*, 2017, **4**, 1600484.
- 44 S. Kuila, K. V. Rao, S. Garain, P. K. Samanta, S. Das, S. K. Pati, M. Eswaramoorthy and S. J. George, *Angew. Chem., Int. Ed.*, 2018, **57**, 17115–17119.